Science
AAAS

Electric Field Effect in Atomically Thin Carbon Films
K. S. Novoselov, *et al.*
Science **306**, 666 (2004);
DOI: 10.1126/science.1102896

Table 1. Conditional probabilities $P(I|S)$ to detect the idler photon in state I given detection of the signal photon in state S, at the point of maximum correlation for Δt = 100 ns delay between read and write pulses; all the errors are based on counting statistics of coincidence events.

Basis	$P(H_i\|H_s)$	$P(V_i\|H_s)$	$P(V_i\|V_s)$	$P(H_i\|V_s)$
0°	0.92 ± 0.02	0.08 ± 0.02	0.88 ± 0.03	0.12 ± 0.03
45°	0.75 ± 0.02	0.25 ± 0.02	0.81 ± 0.02	0.19 ± 0.02

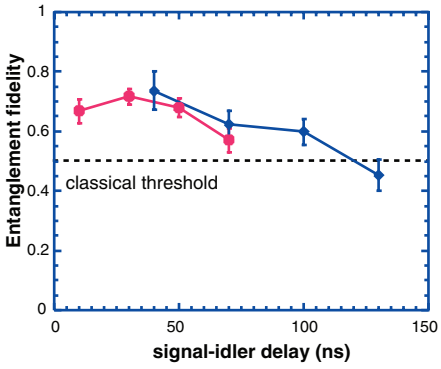

Fig. 4. Time-dependent entanglement fidelity of the signal and the idler F_{si}; circles for Δt = 100 ns, diamonds for Δt = 200 ns.

tection efficiency for the read beam is $\beta \cong 0.04$, so we infer the efficiency of quantum state transfer from the atoms onto the photon, $\xi \cong 0.03$.

We have realized a quantum node by combining the entanglement of atomic and photonic qubits with the atom-photon quantum state transfer. By implementing the second node at a different location and performing a joint detection of the signal photons from the two nodes, the quantum repeater protocol (*11*), as well as distant teleportation of an atomic qubit, may be realized. Based on this work, we estimate the rate for these protocols to be $R_2 \cong (\beta\xi\alpha n_s)^2 R \cong 3 \times 10^{-7} s^{-1}$. However, improvements in ξ that are based on increasing the optical thickness of atomic samples (*16*), as well as elimination of transmission losses, could provide several orders of magnitude increase in R_2. Our results also demonstrate the possibility of realizing quantum nodes consisting of multiple atomic qubits by using multiple beams of light. This approach shows promise for implementation of distributed quantum computation (*20*, *21*).

References and Notes

1. I. Chuang, M. Nielsen, *Quantum Computation and Quantum Information* (Cambridge Univ. Press, Cambridge, 2000).
2. S. Haroche, J. M. Raimond, M. Brune, in *Experimental Quantum Computation and Information*, F. de Martini, C. Monroe, Eds. (Proceedings of the International School of Physics Enrico Fermi, course CXLVIII, IOS Press, Amsterdam, 2002), pp. 37–66.
3. C. A. Sackett *et al.*, *Nature* **404**, 256 (2000).
4. M. D. Barrett *et al.*, *Nature* **429**, 737 (2004).
5. M. Riebe *et al.*, *Nature* **429**, 734 (2004).
6. B. B. Blinov, D. L. Moehring, L.-M. Duan, C. Monroe, *Nature* **428**, 153 (2004).
7. S. Bose, P. L. Knight, M. B. Plenio, V. Vedral, *Phys. Rev. Lett.* **83**, 5158 (1999).
8. H. J. Kimble, *Phys. Scr.* **76**, 127 (1998).
9. A. Kuzmich, E. S. Polzik, in *Quantum Information with Continuous Variables*, S. L. Braunstein, A. K. Pati, Eds. (Kluwer, Dordrecht, 2003).
10. M. D. Lukin, *Rev. Mod. Phys.* **75**, 457 (2003).
11. L.-M. Duan, M. D. Lukin, I. J. Cirac, P. Zoller, *Nature* **414**, 413 (2001).
12. A. Kuzmich *et al.*, *Nature* **423**, 731 (2003).
13. C. H. van der Wal *et al.*, *Science* **301**, 196 (2003).
14. W. Jiang, C. Han, P. Xue, L.-M. Duan, G. C. Guo, *Phys. Rev. A.* **69**, 043819 (2004).
15. C. W. Chou, S. V. Polyakov, A. Kuzmich, H. J. Kimble, *Phys. Rev. Lett.* **92**, 213601 (2004).
16. L.-M. Duan, J. I. Cirac, P. Zoller, *Phys. Rev. A.* **66**, 023818 (2002).
17. A. Kuzmich, T. A. B. Kennedy, *Phys. Rev. Lett.* **92**, 030407 (2004).
18. M. Horodecki, P. Horodecki, R. Horodecki, *Phys. Rev. A.* **60**, 1888 (1994).
19. C. H. Bennett, D. P. DiVincenzo, J. A. Smolin, W. K. Wooters, *Phys. Rev. A.* **54**, 3824 (1996).
20. Y. L. Lim, A. Beige, L. C. Kwek, www.arXiv.org/quant-ph/0408043.
21. S. D. Barrett, P. Kok, www.arXiv.org/quant-ph/0408040.

22. We acknowledge fruitful conversations with T. A. B. Kennedy, J. A. Sauer, L. You, A. Zangwill and, particularly, M. S. Chapman and thank R. Smith and E. T. Neumann for experimental assistance. This work was supported by NASA and the Research Corporation.

28 July 2004; accepted 16 September 2004

Electric Field Effect in Atomically Thin Carbon Films

K. S. Novoselov,[1] A. K. Geim,[1]* S. V. Morozov,[2] D. Jiang,[1] Y. Zhang,[1] S. V. Dubonos,[2] I. V. Grigorieva,[1] A. A. Firsov[2]

We describe monocrystalline graphitic films, which are a few atoms thick but are nonetheless stable under ambient conditions, metallic, and of remarkably high quality. The films are found to be a two-dimensional semimetal with a tiny overlap between valence and conductance bands, and they exhibit a strong ambipolar electric field effect such that electrons and holes in concentrations up to 10^{13} per square centimeter and with room-temperature mobilities of ~10,000 square centimeters per volt-second can be induced by applying gate voltage.

The ability to control electronic properties of a material by externally applied voltage is at the heart of modern electronics. In many cases, it is the electric field effect that allows one to vary the carrier concentration in a semiconductor device and, consequently, change an electric current through it. As the semiconductor industry is nearing the limits of performance improvements for the current technologies dominated by silicon, there is a constant search for new, nontraditional materials whose properties can be controlled by the electric field. The most notable recent examples of such materials are organic conductors (*1*) and carbon nanotubes (*2*). It has long been tempting to extend the use of the field effect to metals [e.g., to develop all-metallic transistors that could be scaled down to much smaller sizes and would consume less energy and operate at higher frequencies than traditional semiconducting devices (*3*)]. However, this would require atomically thin metal films, because the electric field is screened at extremely short distances (<1 nm) and bulk carrier concentrations in metals are large compared to the surface charge that can be induced by the field effect. Films so thin tend to be thermodynamically unstable, becoming discontinuous at thicknesses of several nanometers; so far, this has proved to be an insurmountable obstacle to metallic electronics, and no metal or semimetal has been shown to exhibit any notable (>1%) field effect (*4*).

We report the observation of the electric field effect in a naturally occurring two-dimensional (2D) material referred to as few-layer graphene (FLG). Graphene is the name given to a single layer of carbon atoms densely packed into a benzene-ring structure, and is widely used to describe properties of many carbon-based materials, including graphite, large fullerenes, nanotubes, etc. (e.g., carbon nanotubes are usually thought of as graphene sheets rolled up into nanometer-sized cylinders) (*5*–*7*). Planar graphene itself has been presumed not to exist in the free state, being unstable with respect to the formation of curved structures such as soot, fullerenes, and nanotubes (*5*–*14*).

[1]Department of Physics, University of Manchester, Manchester M13 9PL, UK. [2]Institute for Microelectronics Technology, 142432 Chernogolovka, Russia.

*To whom correspondence should be addressed. E-mail: geim@man.ac.uk

We have been able to prepare graphitic sheets of thicknesses down to a few atomic layers (including single-layer graphene), to fabricate devices from them, and to study their electronic properties. Despite being atomically thin, the films remain of high quality, so that 2D electronic transport is ballistic at submicrometer distances. No other film of similar thickness is known to be even poorly metallic or continuous under ambient conditions. Using FLG, we demonstrate a metallic field-effect transistor in which the conducting channel can be switched between 2D electron and hole gases by changing the gate voltage.

Our graphene films were prepared by mechanical exfoliation (repeated peeling) of small mesas of highly oriented pyrolytic graphite (*15*). This approach was found to be highly reliable and allowed us to prepare FLG films up to 10 μm in size. Thicker films ($d \geq 3$ nm) were up to 100 μm across and visible by the naked eye. Figure 1 shows examples of the prepared films, including single-layer graphene [see also (*15*)]. To study their electronic properties, we processed the films into multiterminal Hall bar devices placed on top of an oxidized Si substrate so that a gate voltage V_g could be applied. We have studied more than 60 devices with $d < 10$ nm. We focus on the electronic properties of our thinnest (FLG) devices, which contained just one, two, or three atomic layers (*15*). All FLG devices exhibited essentially identical electronic properties characteristic for a 2D semimetal, which differed from a more complex (2D plus 3D) behavior observed for thicker, multilayer graphene (*15*) as well as from the properties of 3D graphite.

In FLG, the typical dependence of its sheet resistivity ρ on gate voltage V_g (Fig. 2) exhibits a sharp peak to a value of several kilohms and decays to ~100 ohms at high V_g (note that 2D resistivity is given in units of ohms rather than ohms × cm as in the 3D case). Its conductivity $\sigma = 1/\rho$ increases linearly with V_g on both sides of the resistivity peak (Fig. 2B). At the same V_g where ρ has its peak, the Hall coefficient R_H exhibits a sharp reversal of its sign (Fig. 2C). The observed behavior resembles the ambipolar field effect in semiconductors, but there is no zero-conductance region associated with the Fermi level being pinned inside the band gap.

Our measurements can be explained quantitatively by a model of a 2D metal with a small overlap δε between conductance and valence bands (*15*). The gate voltage induces a surface charge density $n = \varepsilon_0 \varepsilon V_g / te$ and, accordingly, shifts the position of the Fermi energy ε_F. Here, ε_0 and ε are the permittivities of free space and SiO_2, respectively; e is the electron charge; and t is the thickness of our SiO_2 layer (300 nm). For typical $V_g = 100$ V, the formula yields $n \approx 7.2 \times 10^{12}$ cm^{-2}. The electric field doping transforms the shallow-overlap semimetal into either completely electron or completely hole conductor through a mixed state where both electrons and holes are present (Fig. 2). The three regions of electric field doping are clearly seen on both experimental and theoretical curves. For the regions with only electrons or holes left, R_H decreases with increasing carrier concentration in the usual way, as $1/ne$. The resistivity also follows the standard dependence $\rho^{-1} = \sigma = ne\mu$ (where μ is carrier mobility). In the mixed state, σ changes little with V_g, indicating the substitution of one type of carrier with another, while the Hall coefficient reverses its sign, reflecting the fact that R_H is proportional to

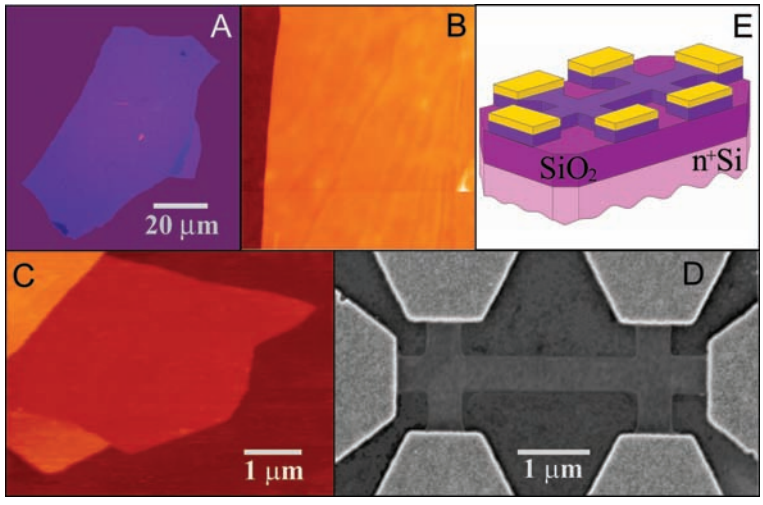

Fig. 1. Graphene films. (**A**) Photograph (in normal white light) of a relatively large multilayer graphene flake with thickness ~3 nm on top of an oxidized Si wafer. (**B**) Atomic force microscope (AFM) image of 2 μm by 2 μm area of this flake near its edge. Colors: dark brown, SiO_2 surface; orange, 3 nm height above the SiO_2 surface. (**C**) AFM image of single-layer graphene. Colors: dark brown, SiO_2 surface; brown-red (central area), 0.8 nm height; yellow-brown (bottom left), 1.2 nm; orange (top left), 2.5 nm. Notice the folded part of the film near the bottom, which exhibits a differential height of ~0.4 nm. For details of AFM imaging of single-layer graphene, see (*15*). (**D**) Scanning electron microscope image of one of our experimental devices prepared from FLG. (**E**) Schematic view of the device in (D).

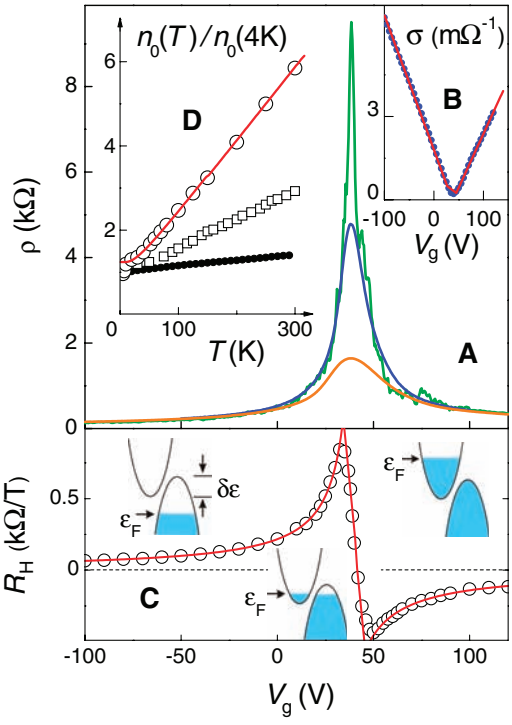

Fig. 2. Field effect in FLG. (**A**) Typical dependences of FLG's resistivity ρ on gate voltage for different temperatures (T = 5, 70, and 300 K for top to bottom curves, respectively). (**B**) Example of changes in the film's conductivity $\sigma = 1/\rho(V_g)$ obtained by inverting the 70 K curve (dots). (**C**) Hall coefficient R_H versus V_g for the same film; T = 5 K. (**D**) Temperature dependence of carrier concentration n_0 in the mixed state for the film in (A) (open circles), a thicker FLG film (squares), and multilayer graphene ($d \approx 5$ nm; solid circles). Red curves in (B) to (D) are the dependences calculated from our model of a 2D semimetal illustrated by insets in (C).

the difference between electron and hole concentrations.

Without electric field doping (at zero V_g), FLG was found to be a hole metal, which is seen as a shift of the peak in ρ to large positive V_g. However, this shift is attributed to an unintentional doping of the films by absorbed water (*16*, *17*). Indeed, we found that it was possible to change the position of the peak by annealing our devices in vacuum, which usually resulted in shifting of the peak close to zero voltages. Exposure of the annealed films to either water vapor or NH_3 led to their p- and n-doping, respectively (*15*). Therefore, we believe that intrinsic FLG is a mixed-carrier material.

Carrier mobilities in FLG were determined from field-effect and magnetoresistance measurements as $\mu = \sigma(V_g)/en(V_g)$ and $\mu = R_H/\rho$, respectively. In both cases, we obtained the same values of μ, which varied from sample to sample between 3000 and 10,000 $cm^2/V{\cdot}s$. The mobilities were practically independent of absolute temperature *T*, indicating that they were still limited by scattering on defects. For $\mu \approx 10{,}000\ cm^2/V{\cdot}s$ and our typical $n \approx 5 \times 10^{12}\ cm^{-2}$, the mean free path is ~0.4 μm, which is surprising given that the 2D gas is at most a few Å away from the interfaces. However, our findings are in agreement with equally high μ observed for intercalated graphite (*5*), where charged dopants are located next to graphene sheets. Carbon nanotubes also exhibit very high μ, but this is commonly attributed to the suppression of scattering in the 1D case. Note that for multilayer graphene, we observed mobilities up to ~15,000 $cm^2/V{\cdot}s$ at 300 K and ~60,000 $cm^2/V{\cdot}s$ at 4 K.

Despite being essentially gigantic fullerene molecules and unprotected from the environment, FLG films exhibit pronounced Shubnikov–de Haas (ShdH) oscillations in both longitudinal resistivity ρ_{xx} and Hall resistivity ρ_{xy} (Fig. 3A), serving as another indicator of the quality and homogeneity of the experimental system. Studies of ShdH oscillations confirmed that electronic transport in FLG was strictly 2D, as one could reasonably expect, and allowed us to fully characterize its charge carriers. First, we carried out the standard test and measured ShdH oscillations for various angles θ between the magnetic field and the graphene films. The oscillations depended only on the perpendicular component of the magnetic field $B{\cdot}\cos\theta$, as expected for a 2D system. More important, however, we found a linear dependence of ShdH oscillations' frequencies B_F on V_g (Fig. 3B), indicating that the Fermi energies ε_F of holes and electrons were proportional to their concentrations *n*. This dependence is qualitatively different from the 3D dependence $\varepsilon_F \propto n^{2/3}$ and proves the 2D nature of charge carriers in FLG. Further analysis (*15*) of ShdH oscillations showed that only a single spatially quantized 2D subband was occupied up to the maximum concentrations achieved in our experiments ($\sim 3 \times 10^{13}\ cm^{-2}$). It could be populated either by electrons with mass $m_e \approx 0.06 m_0$ (where m_0 is the free electron mass) located in two equivalent valleys, or by light and heavy holes with masses of $\sim 0.03 m_0$ and $\sim 0.1 m_0$ and the double-valley degeneracy. These properties were found to be the same for all FLG films studied and are notably different from the electronic structure of both multilayer graphene (*15*) and bulk graphite (*5*–*7*). Note that graphene is expected (*5*–*7*) to have the linear energy dispersion and carriers with zero mass, and the reason why the observed behavior is so well described by the simplest free-electron model remains to be understood (*15*).

We also determined the band overlap δε in FLG, which varied from 4 to 20 meV for different samples, presumably indicating a different number of graphene layers involved (*18*). To this end, we first used a peak value ρ_m of resistivity to calculate typical carrier concentrations in the mixed state, n_0 (e.g., at low *T* for the sample in Fig. 2, A to C, with $\mu \approx 4000\ cm^2/V$ and $\rho_m \approx 8$ kilohms, n_0 was $\sim 2 \times 10^{11}\ cm^{-2}$). Then, δε can be estimated as n_0/D, where $D = 2m_e/\pi\hbar^2$ is the 2D density of electron states and ħ is Planck's constant divided by 2π. For the discussed sample, this yields $\delta\varepsilon \approx 4$ meV [i.e., much smaller than the overlap in 3D graphite (~40 meV)]. Alternatively, δε could be calculated from the temperature dependence of n_0, which characterizes relative contributions of intrinsic and thermally excited carriers. For a 2D semimetal, $n_0(T)$ varies as $n_0(0\ K){\cdot}f\ln[1 + \exp(1/f)]$, where $f = 2k_BT/\delta\varepsilon$ and k_B is Boltzmann's constant; Fig. 2D shows the best fit to this dependence, which yields $\delta\varepsilon \approx 6$ meV. Different FLG devices were found to exhibit a ratio of $n_0(300\ K)/n_0(0)$ between 2.5 and 7, whereas for multilayer graphene it was only ~1.5 (Fig. 2D). This clearly shows that δε decreases with decreasing number of graphene layers. The observed major reduction of δε is in agreement with the fact that single-layer graphene is in theory a zero-gap semiconductor (*5*, *18*).

Graphene may be the best possible metal for metallic transistor applications. In addition to the scalability to true nanometer sizes envisaged for metallic transistors, graphene also offers ballistic transport, linear current-voltage (*I*-*V*) characteristics, and huge sustainable currents ($>10^8\ A/cm^2$) (*15*). Graphene transistors show a rather modest on-off resistance ratio (less than ~30 at 300 K; limited because

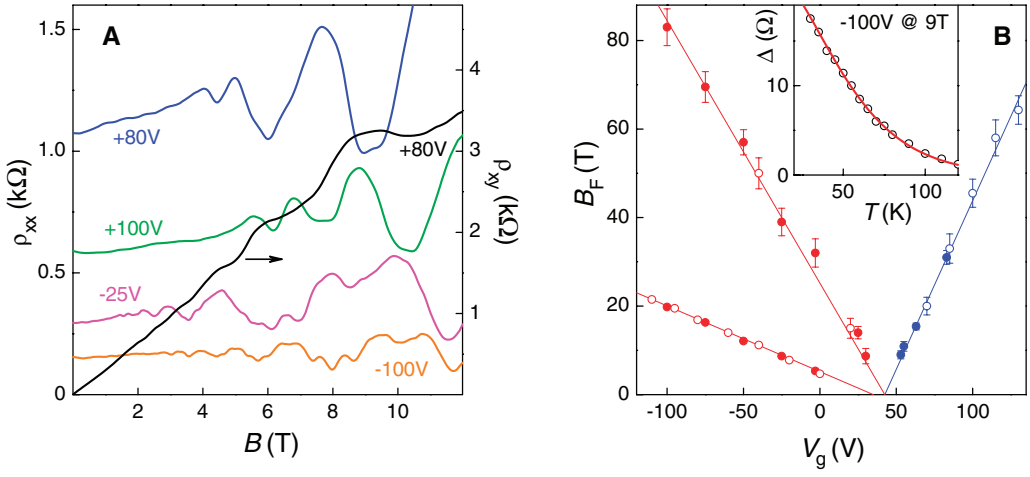

Fig. 3. (**A**) Examples of ShdH oscillations for one of our FLG devices for different gate voltages; *T* = 3 K, and *B* is the magnetic field. As the black curve shows, we often observed pronounced plateau-like features in ρ_{xy} at values close to $(h/4e^2)/\nu$ (in this case, ε_F matches the Landau level with filling factor ν = 2 at around 9 T). Such not-fully-developed Hall plateaus are usually viewed as an early indication of the quantum Hall effect in the situations where ρ_{xx} does not yet reach the zero-resistance state. (**B**) Dependence of the frequency of ShdH oscillations B_F on gate voltage. Solid and open symbols are for samples with $\delta\varepsilon \approx 6$ meV and 20 meV, respectively. Solid lines are guides to the eye. The linear dependence $B_F \propto V_g$ indicates a constant (2D) density of states (*15*). The observed slopes (solid lines) account for the entire external charge *n* induced by gate voltage, confirming that there are no other types of carriers and yielding the double-valley degeneracy for both electrons and holes (*15*). The inset shows an example of the temperature dependence of amplitude Δ of ShdH oscillations (circles), which is fitted by the standard dependence $T/\sinh(2\pi^2k_BT/\hbar\omega_c)$ where ω_c is their cyclotron frequency. The fit (solid curve) yields light holes' mass of $0.03m_0$.

of thermally excited carriers), but this is a fundamental limitation for any material without a band gap exceeding k_BT. Nonetheless, such on-off ratios are considered sufficient for logic circuits (*19*), and it is feasible to increase the ratio further by, for example, using p-n junctions, local gates (*3*), or the point contact geometry. However, by analogy to carbon nanotubes (*2*), other, nontransistor applications of this atomically thin material ultimately may prove to be the most exciting.

References and Notes

1. C. D. Dimitrakopoulos, D. J. Mascaro, *IBM J. Res. Dev.* **45**, 11 (2001).
2. R. H. Baughman, A. A. Zakhidov, W. A. de Heer, *Science* **297**, 787 (2002).
3. S. V. Rotkin, K. Hess, *Appl. Phys. Lett.* **84**, 3139 (2004).
4. A. V. Butenko, D. Shvarts, V. Sandomirsky, Y. Schlesinger, *J. Appl. Phys.* **88**, 2634 (2000).
5. M. S. Dresselhaus, G. Dresselhaus, *Adv. Phys.* **51**, 1 (2002).
6. I. L. Spain, in *Chemistry and Physics of Carbon*, P. L. Walker, P. A. Thrower, Eds. (Dekker, New York, 1981), pp. 119–304.
7. O. A. Shenderova, V. V. Zhirnov, D. W. Brenner, *Crit. Rev. Solid State Mater. Sci.* **27**, 227 (2002).
8. A. Krishnan *et al.*, *Nature* **388**, 451 (1997).
9. E. Dujardin, T. Thio, H. Lezec, T. W. Ebbesen, *Appl. Phys. Lett.* **79**, 2474 (2001).
10. H. Shioyama, *J. Mat. Sci. Lett.* **20**, 499 (2001).
11. Other methods of preparing thin graphitic layers exist. The closest analogs of FLG are nanometer-sized patches of graphene on top of pyrolytic graphite (*12*, *13*), carbon films grown on single-crystal metal substrates (*14*), and mesoscopic graphitic disks with thickness down to ~60 graphene layers (*8*, *9*).
12. A. M. Affoune *et al.*, *Chem. Phys. Lett.* **348**, 17 (2001).
13. K. Harigaya, Y. Kobayashi, K. Takai, J. Ravier, T. Enoki, *J. Phys. Cond. Matter* **14**, L605 (2002).
14. T. A. Land, T. Michely, R. J. Behm, J. C. Hemminger, G. Comsa, *Surf. Sci.* **264**, 261 (1992).
15. See supporting data on *Science* Online.
16. J. Kong *et al.*, *Science* **287**, 622 (2000).
17. M. Krüger, I. Widner, T. Nussbaumer, M. Buitelaar, C. Schönenberger, *N. J. Phys.* **5**, 138 (2003).
18. We believe that our thinnest FLG samples (as in Fig. 2A) are in fact zero-gap semiconductors, because small nonzero values of $\delta\varepsilon$ found experimentally can be attributed to inhomogeneous doping, which smears the zero-gap state over a small range of V_g and leads to finite apparent $\delta\varepsilon$.
19. M. R. Stan, P. D. Franzon, S. C. Goldstein, J. C. Lach, M. M. Zeigler, *Proc. IEEE* **91**, 1940 (2003).

20. Supported by the UK Engineering and Physical Sciences Research Council and the Russian Academy of Sciences (S.V.M., S.V.D.). We thank L. Eaves, E. Hill, and O. Shklyarevskii for discussions and interest.

Supporting Online Material

www.sciencemag.org/cgi/content/full/306/5696/666/DC1
Materials and Methods
SOM Text
Figs. S1 to S11
References and Notes

19 July 2004; accepted 15 September 2004

Hydrated Electron Dynamics: From Clusters to Bulk

A. E. Bragg,[1] J. R. R. Verlet,[1] A. Kammrath,[1] O. Cheshnovsky,[2] D. M. Neumark[1,3]*

The electronic relaxation dynamics of size-selected $(H_2O)_n^-/(D_2O)_n^-$ [$25 \leq n \leq 50$] clusters have been studied with time-resolved photoelectron imaging. The excess electron (e_c^-) was excited through the $e_c^-(p) \leftarrow e_c^-(s)$ transition with an ultrafast laser pulse, with subsequent evolution of the excited state monitored with photodetachment and photoelectron imaging. All clusters exhibited p-state population decay with concomitant s-state repopulation (internal conversion) on time scales ranging from 180 to 130 femtoseconds for $(H_2O)_n^-$ and 400 to 225 femtoseconds for $(D_2O)_n^-$; the lifetimes decrease with increasing cluster sizes. Our results support the "nonadiabatic relaxation" mechanism for the bulk hydrated electron (e_{aq}^-), which invokes a 50-femtosecond $e_{aq}^-(p) \rightarrow e_{aq}^-(s^\dagger)$ internal conversion lifetime.

A free electron introduced into a polar solvent, such as water (*1*) or ammonia (*2*), may be trapped by locally oriented solvent molecules. In water, an "equilibrated" hydrated electron [$e_{aq}^-(s)$] can be transiently confined within a roughly spherical cavity defined by six OH bonds oriented toward the negative charge distribution in the so-called Kevan geometry (*3*–*5*). The hydrated electron is an important reagent in condensed-phase chemistry and molecular biology, as it participates in radiation chemistry, electron transfer, and charge-induced reactivity. Thus, research investigating the dynamics of this species, whether in the presence or absence of other reagents, has attracted considerable attention in the theoretical and experimental physical chemistry communities. Here, we present time-resolved results on the electronic relaxation dynamics of anionic clusters of water that lend profound insight to the elucidation of hydrated electron dynamics in the bulk.

The electronic energetics of a hydrated electron are characterized by three types of states (Fig. 1A): a localized $e_{aq}^-(s)$ ground state; three localized, near-degenerate $e_{aq}^-(p)$ excited states; and a delocalized conduction band (CB) characterized by a charge distribution spread across hundreds of molecules in the solvent "network." The visible absorption spectrum of the equilibrium hydrated electron, a broad band peaking at 720 nm (*1*), is well understood as an excitation from the occupied $e_{aq}^-(s)$ state to the vacant $e_{aq}^-(p)$ states (*4*, *5*). The electron-solvent dynamics subsequent to $e_{aq}^-(p) \leftarrow e_{aq}^-(s)$ excitation are more controversial, however, in spite of considerable experimental (*6*–*12*) and theoretical (*13*, *14*) effort devoted to this problem.

Transient absorption measurements made with femtosecond (fs) laser pulses as short as 5 fs (*12*) show a near infrared (NIR) absorption band beyond 900 nm developing on a 40- to 50-fs time scale after $e_{aq}^-(p) \leftarrow e_{aq}^-(s)$ excitation. This broad feature shifts back to shorter wavelengths on a time scale of several hundred fs, with recovery of the original $e_{aq}^-(s)$ absorption spectrum largely complete within ~1 picosecond (ps). Deuteration of the solvent (*8*, *12*) appears only to affect the fastest measured time scale (i.e., the buildup time of the transient NIR absorption), with τ_{D_2O}/τ_{H_2O} = 1.4 to 1.6. As described by Yokoyama *et al.* (*8*), two rather different energy relaxation mechanisms have been proposed to account for these observations. In the "adiabatic solvation" scheme (*13*, *14*), the infrared transient at the earliest times is attributed to absorption of the $e_{aq}^-(p)$ electron, which is solvated on the upper state within 50 fs (process x in Fig. 1A). The excited electron then undergoes internal conversion (IC) to the ground state (y) on a 400-fs time scale, generating ground-state electrons that further relax on the ~1-ps time scale by dissipating energy to the solvent. In contrast, the "nonadiabatic relaxation" mechanism (*7*, *9*, *12*) invokes much more rapid IC, on a 50-fs time scale, and attributes the transient NIR band at early times to absorption of the ground-state electron in a vibrationally excited solvent environment. In this model, subsequent dynamics are assigned to reorganization of the local (~400 fs) and extended (~1 ps) solvent network following the electronic decay.

We present an alternative and complementary approach to assessing the relaxation dynamics of the hydrated electron through time-resolved photoelectron imaging (TRPEI) studies (*15*) of electron dynamics in size-selected water cluster anions, $(H_2O)_n^-$ and $(D_2O)_n^-$, with $25 \leq n \leq 50$. Water cluster anions were first detected mass spectromet-

[1]Department of Chemistry, University of California, Berkeley, CA 94720, USA. [2]School of Chemistry, The Sackler Faculty of Exact Sciences, Tel-Aviv University, 69978 Israel. [3]Chemical Sciences Division, Lawrence Berkeley National Laboratory, Berkeley, CA 94720, USA.

*To whom correspondence should be addressed. E-mail: dan@radon.cchem.berkeley.edu